Adsorption 11: 295–314, 2005

Further Validation of the Quartic Concentration Profile Approximation for Describing Intraparticle Transport in Cyclic Adsorption Processes

SARANG A. GADRE, ARMIN D. EBNER AND JAMES A. RITTER*
Department of Chemical Engineering, Swearingen Engineering Center, University of South Carolina, Columbia, South Carolina 29208
ritter@engr.sc.edu

Abstract. Models developed previously by the authors that describe nonlinear adsorption, and simultaneous pore and surface diffusion in a single particle, that are based on intraparticle quartic and parabolic concentration profile approximations, and that utilize the summation of the gas and adsorbed phases approach in the material balance formulations, were further validated under more diverse, yet more realistic, cycling conditions. Periodic square, sinusoidal and triangular wave functions were used to more accurately represent the periodic boundary conditions that the external surface of an adsorbent particle may be exposed to during repeated adsorption and desorption cycles in a fixed bed adsorber. Analytical solutions that describe the periodic uptake and release of the adsorbate by the adsorbent were obtained for all three periodic wave functions, and for both the quartic and parabolic profile approximations. By comparing the predictions obtained from both models with the exact numerical solution, the superiority of the quartic model over the parabolic model was clearly demonstrated for all wave functions, and for a wide range of adsorbate-adsorbent systems and bulk concentrations. Excellent agreement between the quartic and exact models was obtained in most cases. In general, the predictions improved as the wave function changed more gradually with time (triangular more gradual than sinusoidal and sinusoidal more gradual than square), as the degree of mathematical linearity of the adsorbate-adsorbent system increased, and as the maximum external surface concentration decreased (an isotherm nonlinearity effect). Subtle differences in the predictive ability of the new approximate models, stemming from the use of the different wave functions, were exposed. Overall, these results exemplify the importance of comparing the predictive ability of new approximate models that describe intraparticle transport under more diverse cycling conditions than are typically utilized in the literature, which has been dominated by the square wave function.

Keywords: linear driving force, LDF, simultaneous pore and surface diffusion, Langmuir isotherm, quartic concentration profile, parabolic concentration profile, cyclic adsorption

Introduction

Approximate models that accurately describe intraparticle adsorption and diffusion in porous adsorbents are continually being sought. This interest stems from their use, not only in simplifying the simulation of fixed bed adsorption processes, such as pressure swing adsorption (PSA), but also in elucidating the controlling transport mechanism, such as pore or surface diffusion.

*To whom correspondence should be addressed.

Many different variations of inherently similar approximate models that describe the intraparticle transport in adsorption systems have been reported in the literature, with their similarity arising from the use of a linear driving force (LDF) approximation first proposed by Glueckauf (1955), or some modified version of this LDF approximation based on the work of Liaw et al. (1979).

Liaw et al. (1979) was the first to show that the LDF approximation of Glueckauf (1955) could be obtained by assuming the adsorbed phase concentration

profile inside the particle to be parabolic. The idea that the mathematics associated with intraparticle transport could be greatly simplified merely by representing the intraparticle concentration profile with a simple parabolic function was quite insightful. So much so that it spawned the development of numerous models that all attempt to simplify the intraparticle diffusion process by taking advantageous of various concentration profile approximations that make the mathematics more tractable.

Parabolic (Do and Rice, 1986, 1955; Do and Mayfield, 1987; Tomida and McCoy, 1987; Do and Nguyen, 1988; Buzanowski and Yang, 1989; Buzanowski and Yang, 1991; Yao and Tien, 1992; Zhang and Ritter, 1997; Botte et al., 1998, 1999; Li and Yang, 1999; Serbezov and Sotirchos, 2001; Gadre and Ritter, 2002a, 2002b), and higher order polynomial (Do and Rice, 1986; Do and Mayfield, 1987; Do and Nguyen, 1988; Buzanowski and Yang, 1989, 1991; Li and Yang, 1999; Serbezov and Sotirchos, 2001; Gadre and Ritter, 2002b) concentration profile approximations have all been examined for mathematical simplification, with the intent of providing reasonable approximations to intraparticle adsorption and diffusion. In some cases, only adsorption uptake in a single particle has been considered using a step or square wave function as the constant boundary condition at the particle surface (Do and Rice, 1986, 1995; Do and Mayfield, 1987; Tomida and McCoy, 1987; Do and Nguyen, 1988; Zhang and Ritter, 1997; Botte et al., 1998; Botte et al., 1999; Gadre and Ritter, 2002a, 2002b). In other cases, both adsorption uptake and desorption release in a single particle have been considered, usually in a cyclic fashion using step or square wave functions (Buzanowski and Yang, 1989, 1991; Serbezov and Sotirchos, 2001), or even more complicated periodic functions like linear and exponential (Serbezov and Sotirchos, 2001). Some of these studies have also developed expressions that describe the uptake in batch adsorbers (Do and Rice, 1995; Yao and Tien, 1992; Li and Yang, 1999). In addition, a few of the cyclic studies have focused on improving these kinds of approximate models for use in very short cycle time situations (Buzanowski and Yang, 1989, 1991; Serbezov and Sotirchos, 2001), like those associated with the simulation of rapid PSA. Although the LDF model (which is always equivalent to assuming a parabolic intraparticle concentration profile) does not perform well in predicting the intraparticle transport for short cycle times (Rodrigues and Dias, 1998), the accuracy of the polynomial concentration profile approximation tends to increase with the degree of the polynomial (Serbezov and Sotirchos, 2001).

Others have recently shown that the LDF approximation provides satisfactory predictions of intraparticle transport over a wide range of conditions during cyclic operation, especially for long cycle times that are typical of most commercial PSA processes (Rodrigues and Dias, 1998; Sircar and Hufton, 2000; Todd and Webley, 2002). In fact, Ritter and co-workers (Zhang and Ritter, 1997; Botte et al., 1998, 1999; Gadre and Ritter, 2002a, 2002b) proposed a novel approach that involved summing together the gas and adsorbed phase concentrations inside the particle and then applying either parabolic (Zhang and Ritter, 1997; Botte et al., 1998, 1999; Gadre and Ritter, 2002a) or quartic (Gadre and Ritter, 2002b) profile approximations to obtain approximate yet more robust modifications of the simple LDF model. Their approach described not only the simultaneous intraparticle pore and surface diffusion transport, but it also accounted for adsorption isotherm nonlinearity (Zhang and Ritter, 1997; Botte et al., 1998, 1999; Gadre and Ritter, 2002a, 2002b). The approach by Ritter and co-workers was also extended to account for a concentration dependent surface diffusivity (Botte et al., 1999; Gadre and Ritter, 2002a, 2002b). In all cases, they obtained analytical expressions for the fractional uptake and intraparticle adsorbed phase concentration profiles, as well as explicit differential expressions for the rate of accumulation in the adsorbed phase that can be used as an accurate simplification in fixed bed adsorption models. However, once again, only square wave functions were used as the surface boundary condition.

The point being made here and elsewhere (Todd and Webley, 2002) is subtle but important, as it deals with the fact that in reality an adsorbent particle hardly ever experiences a step change at its surface, with the magnitude corresponding to the feed concentration, especially after achieving periodic behavior. As shown recently by Todd and Webley (2002) the sole use of a square wave function has resulted in some serious errors in the predictive ability of the expressions and correlations developed for the cycle time dependence of the LDF mass transfer coefficient when compared to the exact numerical analyses of, for example, rapid PSA cycles. The same limitations may result when comparing any new approximate model for intraparticle transport to the exact numerical solution when only square wave functions are used.

Therefore, the objective of this study is to further validate the use of the intraparticle quartic concentration profile approximation developed by Gadre and Ritter (2002b) for use in cyclic fixed bed adsorption process modeling. But instead of using just a periodic square wave function to judge the predictive ability of this new approximate model, as done in Gadre and Ritter (2002b) for the case of only adsorption, two additional periodic wave functions, such as sinusoidal and triangular, are used to more accurately represent the periodic boundary condition a particle may be exposed to during repeated adsorption and desorption cycles in a fixed bed adsorber. Periodic analytical solutions are obtained for all three wave functions and for both the quartic and parabolic profile approximations. The superiority of the quartic profile model (Gadre and Ritter, 2002b) over the parabolic profile model (Gadre and Ritter, 2002a) is clearly demonstrated by comparing the fractional periodic uptakes and releases obtained from both models against the exact numerical solution obtained for all three periodic wave functions and for a wide range of adsorbate-adsorbent systems and conditions. Subtle and in some cases misleading differences in the predictive ability of the new approximate model, stemming from the use of the different wave functions, are exposed.

Model Development

The mass balance governing both the gas and adsorbed phases in a spherical adsorbent particle results in the following PDEs in dimensionless form (Zhang and Ritter, 1997):

$$\frac{\partial \psi}{\partial \tau} = -\frac{1}{\xi^2}\frac{\partial(\xi^2 N_\xi)}{\partial \xi} \tag{1}$$

$$N_\xi = -\frac{\partial C}{\partial \xi} - \lambda(Q)\frac{\partial Q}{\partial \xi} \tag{2}$$

where $\tau = D_g t/R_p^2 \quad \xi = r/R_p, C = c/c_{s,\max}, Q = \gamma q/c_{s,\max}, \gamma = \rho_p/\varepsilon_p, \lambda(Q) = D_a(Q)/D_g$ and $\Psi = C + \mathrm{Q}$. ψ represents the total moles in both the gas and adsorbed phases inside the adsorbent particle. The corresponding initial and boundary conditions are

$$\Psi = 0 \quad \text{for } \tau = 0 \tag{3}$$

$$\frac{\partial \Psi}{\partial \xi} = 0 \quad \text{for } \xi = 0 \tag{4}$$

$$\Psi = \Psi_s(\tau) \quad \text{for } \xi = 1 \tag{5}$$

where $\psi_s(\tau)$ represents the cyclic change of the concentration at the external surface of the adsorbent particle, which is represented by periodic functions such as, square, sinusoidal, and triangular wave functions.

As shown in the previous work by Gadre and Ritter (2002b), by taking a volume average of the concentration in the particle, Eq. (1) is transformed into the following ODE as

$$\frac{d\bar{\Psi}}{d\tau} = -3N_\xi|_{\xi=1} \tag{6}$$

with the volume average sum of ψ given by

$$\bar{\Psi} = 3\int_0^1 \Psi \xi^2 d\xi \tag{7}$$

Equation (6) reduces to

$$\frac{d\bar{\Psi}}{d\tau} = 3\kappa \frac{\partial \Psi}{\partial \xi}\bigg|_{\xi=1} \tag{8}$$

by applying the surface boundary condition given in Eq. (5); and κ is defined as

$$\kappa = \frac{(1+\lambda(Q_S(\tau))f'(C)|_{C_S(\tau)})}{(1+f'(C)|_{C_S(\tau)})} \tag{9}$$

in terms of a general adsorption isotherm of the form, $Q = f(C)$. Equation (9) shows that κ must be evaluated at the surface concentration, $Q_S(\tau)$, which changes with time in this cyclic analysis. To obtain an analytical solution, it is assumed that the variation of κ with time is insignificant, and that it can be evaluated at the maximum surface concentration $C_{s,\max}$. The accuracy of this assumption is verified later.

Equation (8) represents the first of the two ODEs that are needed in this analysis. The other ODE is obtained by applying the limit as $\xi \to 0$ to Eq. (1) and using L'Hopital's rule; this results in the following PDE that describes the centerline concentration behavior in the particle:

$$\frac{d\Psi_o}{d\tau} = -3\frac{\partial N_\xi}{\partial \xi}\bigg|_{\xi=0} \tag{10}$$

Similarly, Eq. (10) reduces to

$$\frac{d\Psi_0}{d\tau} = 3\kappa_0 \frac{\partial^2 \Psi}{\partial \xi^2}\bigg|_{\xi=0} \tag{11}$$

where

$$\kappa_0 = \frac{\left(1+\lambda(Q_0(\tau))f'(C)|_{C_0(\tau)}\right)}{\left(1+f'(C)|_{C_0(\tau)}\right)} \tag{12}$$

Equation (11) represents the second ODE that is needed. Again, just as with κ, even though κ_0 varies with time, it is assumed to be essentially constant and simply evaluated at a limiting value, i.e., with the centerline concentrations Q_0 and C_0 assumed to be zero over an entire cycle.

Now, a quartic concentration profile approximation is introduced, which is later differentiated and substituted into the Eqs. (8) and (11); these equations are then solved simultaneously for $\bar{\Psi}$ and Ψ_0. This quartic polynomial function is written as (Rice and Do, 1986)

$$\Psi = A_0(\tau) + A_2(\tau)\xi^2 + A_4(\tau)\xi^4 \tag{13}$$

Differentiating with respect to ξ twice leads to,

$$\left.\frac{\partial \Psi}{\partial \xi}\right|_{\xi=1} = 2A_2(\tau) + 4A_4(\tau) \tag{14}$$

and

$$\left.\frac{\partial^2 \Psi}{\partial \xi^2}\right|_{\xi=0} = 2A_2(\tau) \tag{15}$$

Applying the limit as $\xi \to 0$ to Eq. (13) gives,

$$A_0(\tau) = \Psi_0(\tau) \tag{16}$$

and substituting Eq. (13) into (7) yields,

$$\bar{\Psi} = A_0(\tau) + \frac{3}{5}A_2(\tau) + \frac{3}{7}A_4(\tau) \tag{17}$$

By applying the boundary condition given in Eqs. (5) to (13),

$$\Psi_S(\tau) = A_0(\tau) + A_2(\tau) + A_4(\tau) \tag{18}$$

Eqs. (16), (17) and (18) are now combined to obtain $A_2(\tau)$ and $A_4(\tau)$ as

$$A_2(\tau) = -\frac{5}{6}(4\Psi_0(\tau) + 3\Psi_S(\tau) - 7\bar{\Psi}(\tau)) \tag{19}$$

$$A_4(\tau) = \frac{7}{6}(2\Psi_0(\tau) + 3\Psi_S(\tau) - 5\bar{\Psi}(\tau)) \tag{20}$$

Substituting Eqs. (19) and (20) into Eqs. (14) and (15), and combining these equations with Eqs. (8) and (11) yields,

$$\frac{d\bar{\Psi}}{d\tau} = \kappa(8\Psi_0(\tau) + 27\Psi_S(\tau) - 35\bar{\Psi}(\tau)) \tag{21}$$

and

$$\frac{d\Psi_0}{d\tau} = \kappa_0(-20\Psi_0(\tau) - 15\Psi_S(\tau) + 35\bar{\Psi}(\tau)) \tag{22}$$

with the initial condition for the cyclic process as $\bar{\Psi} = \bar{\Psi}_i$ and $\Psi_0 = \Psi_{0,i}$ at $\tau = \tau_i$. Similarly, for the parabolic profile approximation, the corresponding ODE is given by

$$\frac{d\bar{\Psi}}{d\tau} = 15\kappa(\Psi_S(\tau) - \bar{\Psi}) \tag{23}$$

with the initial condition specified as $\bar{\Psi} = \bar{\Psi}_i$ at $\tau = \tau_i$. What remains to be done is to introduce the periodic functions that describe how the concentration $\Psi_s(\tau)$ changes with time at the external particle surface during cyclic operation.

Square Wave Function

For the case where the surface concentration varies as a simple step function (i.e., a square wave) with time (the most commonly studied case), the surface concentration function $\Psi_s(\tau)$ is represented by

$$\Psi_S(\tau) = \Psi_{S,i} \quad \tau = \tau_i \tag{24a}$$

$$\Psi_S(\tau) = \Psi_{S,f} \quad \tau_i < \tau < \tau_i + \tau_P \tag{24b}$$

where $\Psi_{s,i} = 0$ and $\Psi_{s,f} = \Psi_{s,\max}$ for adsorption and vice versa for desorption. Substituting $\Psi_S(\tau)$ from Eq. (24) into Eqs. (21) and (22) and solving this system of two ODEs analytically for $\bar{\Psi}$ and Ψ_0 yields the following explicit expression for the fractional uptake or release based on the quartic profile approximation

$$\left(\frac{M_t}{M_\infty}\right)_{\text{quar,sqr}} = \frac{\bar{\Psi}}{\Psi_{S,\max}} = A_{sqr_1} + (B_{sqr_1} - B_{sqr_2})\exp(-j_1(\tau - \tau_i)) + \left(B_{sqr_1} + B_{sqr_2}\right)\exp\left(-j_2(\tau - \tau_i)\right) \tag{25}$$

where

$$A_{sqr_1} = \frac{\Psi_{S,f}}{\Psi_{S,\max}} \tag{26}$$

$$B_{sqr_1} = \frac{1}{2}\frac{\bar{\Psi}_i - \Psi_{S,f}}{\Psi_{S,\max}} \tag{27}$$

$$B_{sqr_2} = \frac{5}{2}\frac{(4\kappa_0 - 7\kappa)}{\mu}\frac{(\bar{\Psi}_i - \Psi_{s,f})}{\Psi_{s,\max}} + 8\frac{\kappa}{\mu}\frac{(\Psi_{0,j} - \Psi_{s,f})}{\Psi_{s,\max}} \tag{28}$$

$$j_1 = \frac{1}{2}(35\kappa + 20\kappa_o + \mu) \tag{29}$$

$$j_2 = \frac{1}{2}(35\kappa + 20\kappa_o - \mu) \tag{30}$$

$$\mu = \sqrt{1225\kappa^2 - 280\kappa\kappa_o + 400\kappa_o^2} \tag{31}$$

Similarly, the corresponding expression for the fractional uptake or release based on the parabolic profile approximation is given by

$$\left(\frac{M_t}{M_\infty}\right)_{\text{quar},sqr} = \frac{\bar{\Psi}}{\Psi_{s,\max}} = Ap_{sqr_1} + Ap_{sqr_2}\exp[-15\kappa(\tau - \tau_i)] \tag{32}$$

where

$$Ap_{sqr_1} = \frac{\Psi_{s,f}}{\Psi_{s,\max}} \tag{33}$$

$$Ap_{sqr_2} = \frac{\bar{\Psi}_i - \Psi_{s,f}}{\Psi_{s,\max}} \tag{34}$$

Sinusoidal Wave Function

For the case where the surface concentration varies sinusoidally with time, the surface concentration function $\Psi_s(\tau)$ is represented by

$$\Psi_S(\tau) = \Psi_{S,\max}\sin\left[\frac{\pi}{2}\frac{\tau - \tau_i}{\tau_P} + \omega\right] \quad \tau_i \le \tau < \tau_i + \tau_P \tag{35}$$

where ω is equal to 0 and $\pi/2$ during adsorption and desorption, respectively. Substituting $\Psi_s(\tau)$ from Eq. (35) into Eqs. (21) and (22) and solving this system of two ODEs analytically for $\bar{\Psi}$ and Ψ_0 yields the following explicit expression for the fractional uptake or release based on the quartic profile approximation

$$\left(\frac{M_t}{M_\infty}\right)_{quar,\sin} = \frac{\bar{\Psi}}{\Psi_{S,\max}} = A_{\sin_1}\sin\left[\frac{\pi}{2}\frac{\tau - \tau_i}{\tau_P} + \omega\right] + A_{\sin_2}\cos\left[\frac{\pi}{2}\frac{\tau - \tau_i}{\tau_P} + \omega\right] + (B_{\sin_1} + B_{\sin_2})\exp[-j_1(\tau - \tau_i)] + (B_{\sin_1} - B_{\sin_2})\exp[-j_2(\tau - \tau_i)] \tag{36}$$

where

$$A_{\sin_1} = \frac{15\kappa\left(8\kappa_0 + 11760\kappa\kappa_0^2 + 63\kappa\right)}{\eta^2} \tag{37}$$

$$A_{\sin_2} = \frac{-3\kappa\left(1120\kappa\kappa_0 + 9 + 2800\kappa_0^2\right)}{\eta^2} \tag{38}$$

$$B_{\sin_1} = -\frac{1}{2}\left(A_{\sin_1}\sin\omega + A_{\sin 2}\cos\omega - \frac{\bar{\Psi}_i}{\bar{\Psi}_{S,\max}}\right) \tag{39}$$

$$B_{\sin_2} = \frac{15}{2}\frac{\kappa\left(-2205\kappa^2 - 28\kappa\kappa_0 - 223440\kappa_0^2\kappa^2 + 235200\kappa_0^3\kappa - 160\kappa_0^2\right)}{\eta^2\mu}\sin\omega - \frac{15}{2}\frac{\kappa\left(11200\kappa_0^3 + 20\kappa_0 + 7920\kappa^2\kappa_0 + 560\kappa\kappa_o^2 - 63\kappa\right)}{\eta^2\mu}\cos\omega - \frac{1}{2}\frac{(20\kappa_0 - 35\kappa)\bar{\Psi}_i + 16\kappa\Psi_{0,i}}{\Psi_{S,\max}\mu} \tag{40}$$

$$\eta = \sqrt{1 + \mu^2 + 840\kappa\kappa_o(1 + 210\kappa\kappa_o)} \tag{41}$$

Similarly, the corresponding expression for the fractional uptake or release based on the parabolic profile approximation is given as

$$\left(\frac{M_t}{M_\infty}\right)_{\text{para, sin}} = \frac{\bar{\Psi}}{\Psi_{SS}} = Ap_{\sin_1}\sin\left[\frac{\pi}{2}\frac{\tau - \tau_i}{\tau_P} + \omega\right] + Ap_{\sin_2}\cos\left[\frac{\pi}{2}\frac{\tau - \tau_i}{\tau_P} + \omega\right] + Bp_{\sin_1}\exp[-15\kappa\,(\tau - \tau_i)] \tag{42}$$

where

$$Ap_{\sin_1} = \frac{225\kappa^2}{225\kappa^2 + 1} \tag{43}$$

$$Ap_{\sin_2} = \frac{-15\kappa}{225\kappa^2 + 1} \tag{44}$$

$$Bp_{\sin_1} = \frac{15\kappa\Psi_{S,\max}\cos\omega - 225\kappa^2\Psi_{S,\max}\sin\omega + (225\kappa^2 + 1)\Psi_{P,i}}{(225\kappa^2 + 1)\Psi_{S,\max}} \tag{45}$$

Triangular Wave Function

For the case where the surface concentration varies triangularly with time, the surface concentration function $\Psi_s(\tau)$ is represented by

$$\Psi_S(\tau) = \Psi_{S,i} + a(\tau - \tau_i) \quad \tau_i \le \tau < \tau_i + \tau_P \tag{46}$$

where a is the slope and is equivalent to $\Psi_{s,\max}/\tau_p$ and $-\Psi_{s,\max}/\tau_p$ during adsorption and desorption, respectively. $\Psi_{s,i}$ is the initial surface concentration and set equal to zero and $\Psi_{s,\max}$ during adsorption and desorption, respectively. Substituting $\Psi_s(\tau)$ from Eq. (46) into Eqs. (21) and (22) and solving this system of two ODEs analytically for $\bar{\Psi}$ and Ψ_0 yields the following explicit expression for the fractional uptake (positive slope, a) or release (negative slope, $-a$) based on the quartic profile approximation

$$\left(\frac{M_t}{M_\infty}\right)_{\text{quar},tri} = \frac{\bar{\Psi}}{\Psi_{S,\max}} = A_{tr_1} + A_{tr_2} + A_{tr_3}(\tau - \tau_i) + (B_{tr_1} - B_{tr_2})\exp(-j_1(\tau - \tau_i)) + (B_{tr_1} + B_{tr_2})\exp(-j_2(\tau - \tau_i)) \quad (47)$$

where

$$A_{tr_1} = \frac{\Psi_{S,i}}{\Psi_{S,\max}} \quad (48)$$

$$A_{tr_2} = -\frac{a}{105}\frac{(5\kappa_0 + 2\kappa)}{\kappa\kappa_0\Psi_{S,\max}} \quad (49)$$

$$A_{tr_3} = \frac{a}{\Psi_{S,\max}} \quad (50)$$

$$B_{tr_1} = -\frac{1}{2}A_{tr_1} + \frac{1}{2}\frac{\bar{\Psi}_i - \Psi_{S,i}}{\Psi_{S,\max}} \quad (51)$$

$$B_{tr_2} = \frac{1}{42}\frac{\left(\kappa_0\kappa + 20\kappa_0^2 + 14\kappa^2\right)a}{\kappa\kappa_0\mu\Psi_{S,\max}} + \frac{5}{2}\frac{(4\kappa_0 - 7\kappa)}{\mu}\frac{(\bar{\Psi}_i - \Psi_{S,i})}{\Psi_{S,\max}} + 8\frac{\kappa}{\mu}\frac{(\Psi_{0,i} - \Psi_{S,i})}{\Psi_{S,\max}} \quad (52)$$

Similarly, the corresponding expression for the fractional uptake (positive slope, a) or release (negative slope, $-a$) based on the parabolic profile approximation is given by

$$\left(\frac{M_t}{M_\infty}\right)_{\text{quar},tri} = \frac{\bar{\Psi}}{\Psi_{S,\max}} = \frac{\Psi_{S,i}}{\Psi_{S,\max}} + Ap_{tr_1} + Ap_{tr_2}(\tau - \tau_i) + Bp_{tr_1}\exp[-15\kappa(\tau - \tau_i)] \quad (53)$$

where

$$Ap_{tr_1} = -\frac{a}{15\kappa\Psi_{S,\max}} \quad (54)$$

$$Ap_{tr_2} = \frac{a}{\Psi_{S,\max}} \quad (55)$$

$$Bp_{tr_1} = -Ap_{tr_1} + \frac{\bar{\Psi}_{P,i} - \Psi_{S,i}}{\Psi_{S,\max}} \quad (56)$$

Results and Discussion

For each periodic wave function, the analytical solutions obtained from the quartic profile approximation, referred to as quartic analytical (QA), and those obtained from the parabolic profile approximation, referred to as parabolic analytical (PA), are compared to the exact numerical solution, referred to as exact numerical (EN). The EN solution was obtained by solving the system of equations depicted in Eqs. (1) and (2) numerically, along with the corresponding boundary conditions given in Eqs. (3), (4) and (5). To verify the validity of the assumptions made when using constant values of κ and κ_0, the system of two ordinary differential equations, i.e., Eqs. (21) and (22), along with the definitions of κ and κ_0 provided in Eqs. (9) and (12), were also solved numerically. This model is referred to as quartic numerical (QN). Finally, since Gadre and Ritter (2002a) showed their parabolic profile approximation, which accounts for simultaneous pore and surface diffusion, to always be superior to the LDF approximation, which accounts only for surface diffusion, the LDF model was not investigated in this study.

To reveal the effectiveness of the QA model under periodic conditions, the same three adsorbent-adsorbate systems studied by Gadre and Ritter (2002a, 2002b) were used here. These characteristically different systems include hexane-activated carbon at 298 K, ethane-5A zeolite at 298 K, and methane-activated carbon at 298 K, which represent very strong, moderately strong, and somewhat strong adsorbate-adsorbent systems, respectively. The physical parameters for these systems are provided elsewhere (Botte et al., 1998, 1999), including the Langmuir adsorption isotherm parameters, where the Langmuir isotherm is given by

$$Q = \frac{Q_m b' C}{1 + b' C} \quad (57)$$

$$f'(C)|_{C_s} = Q_m b'\left(1 - \frac{Q_s}{Q_m}\right) \quad (58)$$

Each adsorbate-adsorbent system was studied at three maximum surface concentrations ($c_{s,\max}$)

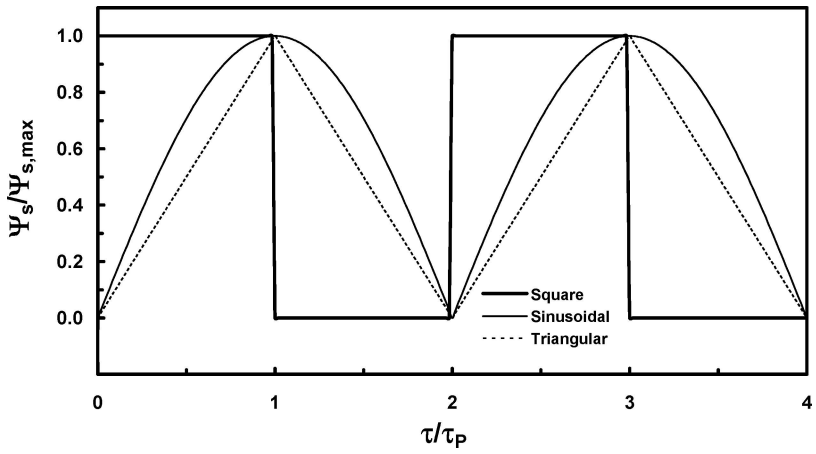

Figure 1. Comparison of the periodic square, sinusoidal and triangular wave functions, where $\tau_P = 1676$, 270 and 3414, respectively, for the hexane-activated carbon, ethane-5A zeolite and methane-activated carbon systems, all at 298 K.

corresponding to 10, 40 and 70% of the adsorbent capacity (q_m) over two complete uptake and release cycles to also examine the effect of isotherm nonlinearity. The periodic behavior of the square, sinusoidal, and triangular wave function surface boundary conditions are shown in Fig. 1. The half cycle time τ_p for each adsorbate-adsorbent system was chosen so that $C_{s,\max}$ was always being approached during adsorption. The resulting periodic uptake (adsorption) and release (desoprtion) curves were used to compare the performances of the QA, QN and PA models with the EN model.

Square Wave Function

In this case, the surface concentration varies squarely with time, as described by the periodic function given in Eq. (24) and shown in Fig. 1. An instantaneous increase in the surface concentration from $\Psi_{s,i} = 0$ to $\Psi_{s,f} = \Psi_{s,\max}$ was imposed as a step change during adsorption, and then after τ_P had elapsed an instantaneous decrease in the surface concentration from $\Psi_{s,i} = \Psi_{s,\max}$ to $\Psi_{s,f} = 0$ was imposed as a step change during desorption. Figures 2, 3 and 4 respectively display the fractional uptake and release curves obtained from the approximate and exact models at maximum surface concentrations ($q_{s,\max}$) corresponding to 10, 40 and 70% of the adsorbent capacity (q_m) for the hexane-activated carbon, ethane-5A zeolite, and methane-activated carbon systems all at 298 K. The corresponding half-cycle times are given in Fig. 1.

The square wave function is definitely the most abruptly changing surface boundary condition studied here. It is also the most widely used periodic function for proving the validity of approximate models, as discussed in detail in the Introduction section. However, it is perhaps the most unrealistic function when it comes to the actual variation in concentration that the surface of an adsorbent particle is exposed to during periodic cycling in fixed bed adsorption processes like PSA. Hence, the ubiquitous use of such a function has the inherent possibility of producing erroneous conclusions about approximate model viability, as illustrated below and in subsequent discussions.

For the very strong adsorbate system shown in Fig. 2, all three approximate models tend to deviate only slightly from the EN model and to about the same degree when attempting to predict the inherently sawtooth response of the step changes during adsorption and desorption. Reasons for this surprisingly good behavior have been given elsewhere (Botte et al., 1998, 1999; Gadre and Ritter, 2002) and stem from the fact that this very strong adsorbate system is mathematically the most linear system considered here (Botte et al., 1998); hence, both the QA and PA models provide reasonably accurate predictions of the EN model over a broad range of maximum surface concentrations even for an abruptly changing square wave function. These results also indicate that it is quite valid to assume κ and κ_0 to be constant for very strong adsorbate systems, even under cyclic conditions.

For the moderately strong adsorbate system shown in Fig. 2, the curve from the QA model overlaps that

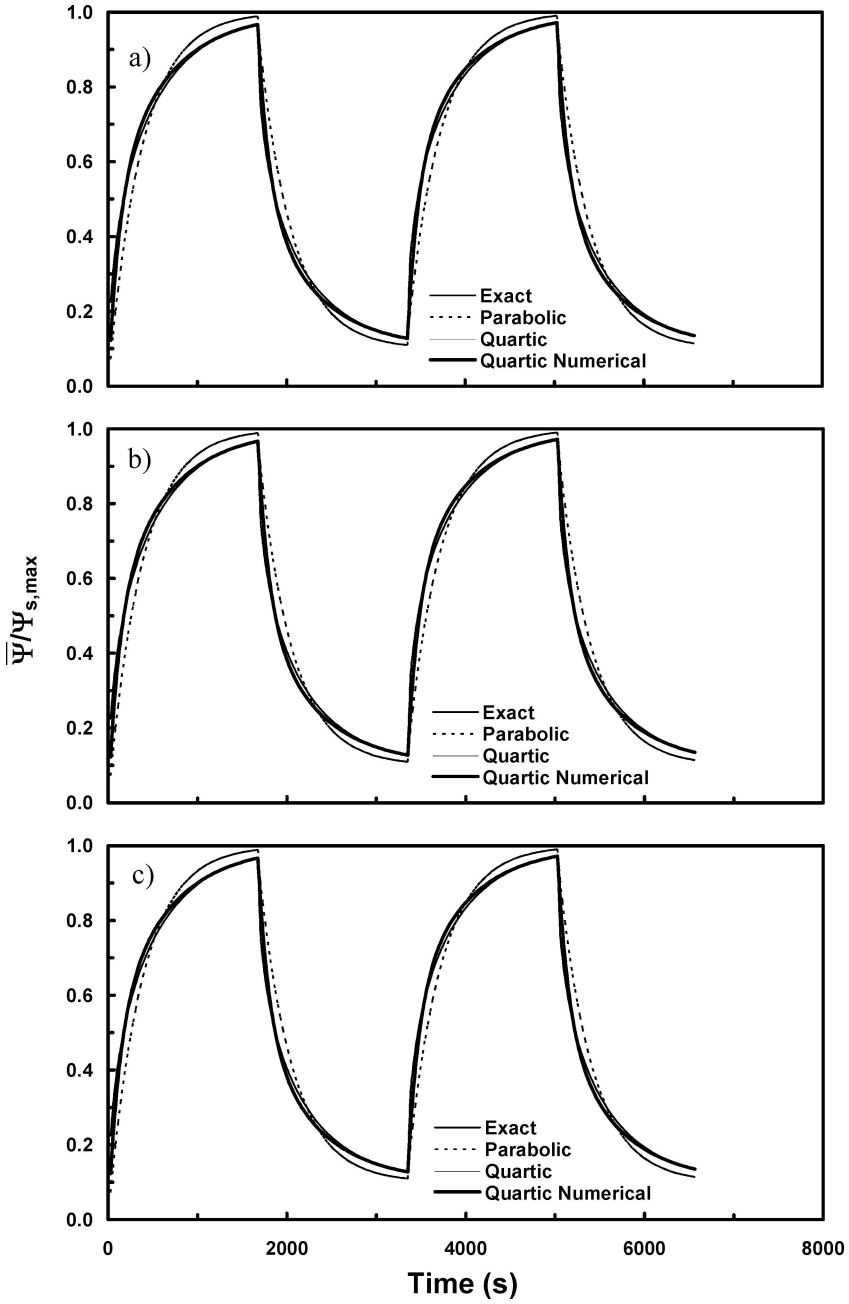

Figure 2. Comparison of fractional uptake curves obtained from various models for a square change in the surface concentration for hexane-activated carbon at 298 K and $q_{s,\max}/q_m$ equal to (a) 0.1, (b) 0.4, and (c) 0.7.

from the EN model only for the lower maximum surface concentration, with deviations clearly increasing as the maximum surface concentration increases. In all cases, the PA model provides the worst predictions, followed by the QA model, and then the QN model. These less than exemplary results are caused by the ethane-5A zeolite system being the most nonlinear system studied here from a mathematical point of view (Botte et al., 1998); hence, the QA and PA models are not expected to predict the fractional uptakes and releases with the same degree of accuracy as the previous system, especially for this square wave function. The fact that

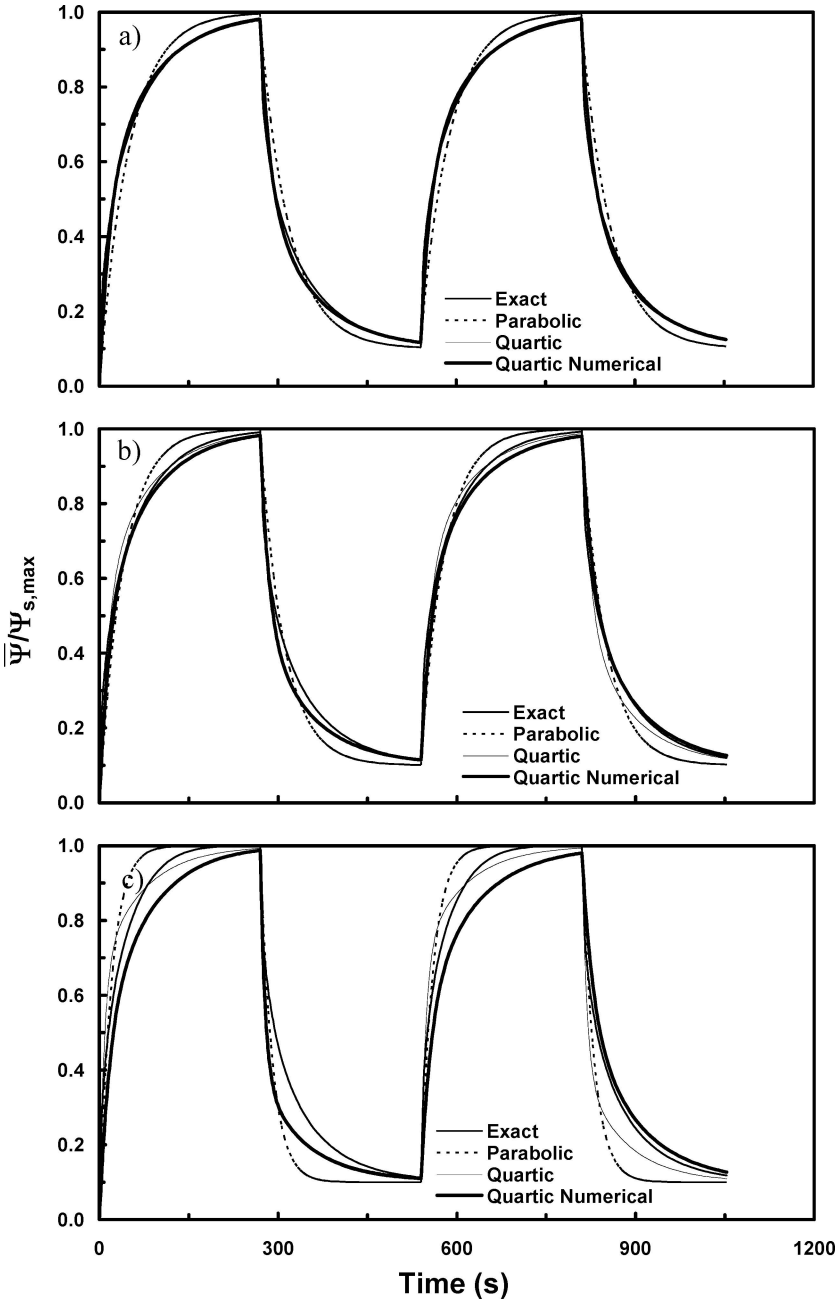

Figure 3. Comparison of fractional uptake curves obtained from various models for a square change in the surface concentration for ethane-5A zeolite at 298 K and $q_{s,\max}/q_m$ equal to (a) 0.1, (b) 0.4, and (c) 0.7.

deviations from the EN model increase with increasing maximum surface concentration is also consistent with these equations becoming more nonlinear (due also to an isotherm nonlinearity effect) as the maximum surface concentration increases. Nevertheless, for all three maximum surface concentrations and over each entire cycle, the QA model always performs better than the PA model, and in most cases the QA model agrees well with the QN model, which essentially overlaps the EN model. This last result justifies the use of constant

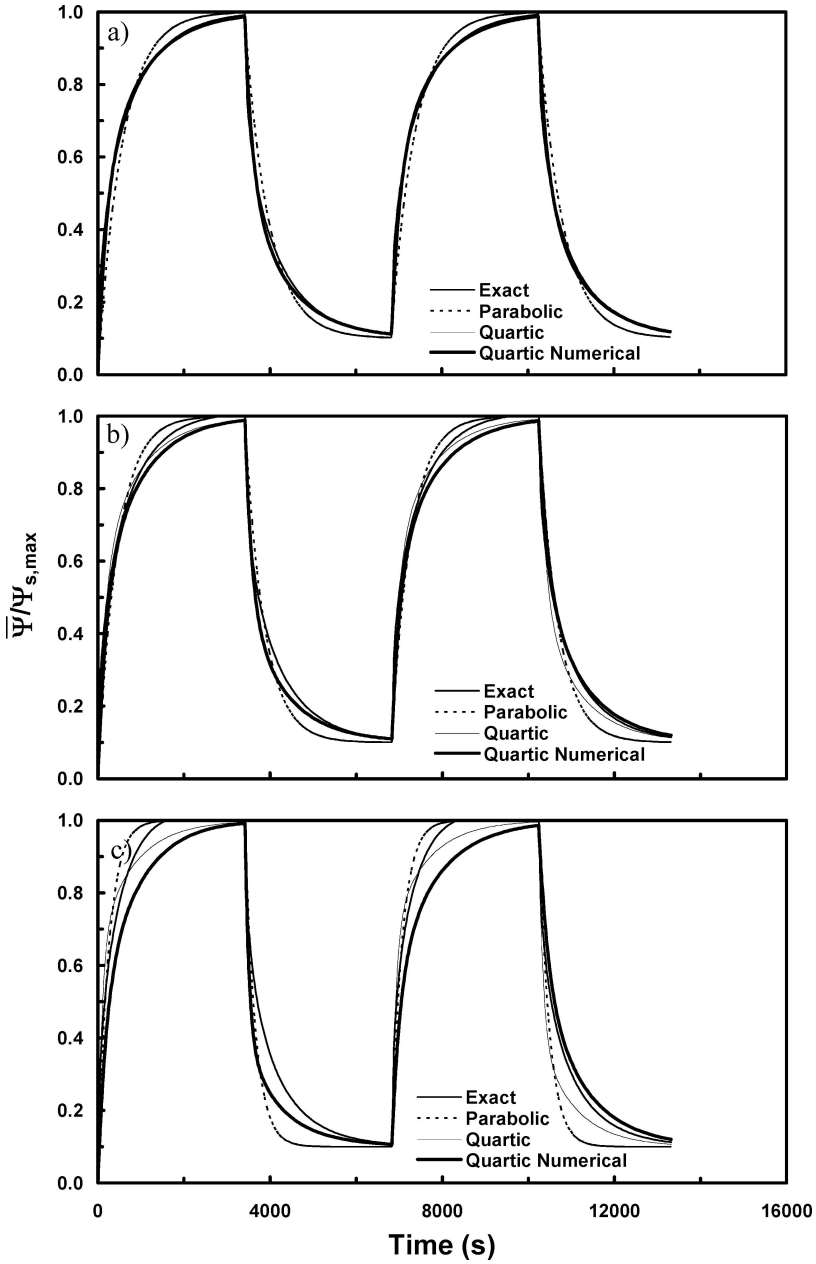

Figure 4. Comparison of fractional uptake curves obtained from various models for a square change in the surface concentration for methane-activated carbon at 298 K and $q_{s,\max}/q_m$ equal to (a) 0.1, (b) 0.4, and (c) 0.7.

values of κ and κ_0, even with marked, mathematically nonlinear systems.

For the somewhat strong adsorbate system shown in Fig. 4, the curve from the QA model now overlaps the EN model for the lower maximum surface concentration; but deviations begin to appear and grow as the maximum surface concentration increases. Although this system represents the weakest adsorbate-adsorbent system considered here, it still exhibits mathematical nonlinearity particularly at higher maximum surface concentrations (Botte et al., 1998). As a result, the PA model deviates substantially from the exact solution,

especially as the maximum surface concentration increases. The QA model always outperforms the PA model, and in most cases, it agrees quite well with the QN model, except for the higher maximum surface concentration. This last result further justifies the use of constant values of κ and κ_0 for systems exhibiting a moderate degree of mathematically nonlinearity.

Sinusoidal Wave Function

In this case, the surface concentration varies sinusoidally with time, as described by the periodic function given in Eq. (35) and shown in Fig. 1. The surface concentration ψ_s increased sinusoidally with time while approaching $\psi_{s,\max}$ during adsorption and decreased sinusoidally with time while approaching zero during desorption. Figures 5, 6 and 7 respectively display the fractional uptake and release curves obtained from the approximate and exact models at maximum surface concentrations ($q_{s,\max}$) corresponding to 10, 40 and 70% of the adsorbent capacity (q_m) for the hexane-activated carbon, ethane-5A zeolite, and methane-activated carbon systems all at 298 K. The corresponding half-cycle times are given in Fig. 1.

The sinusoidal wave function is the second most abruptly changing surface boundary condition studied here, with it exhibiting a rather gradual sinusoidal change over a cycle as shown in Fig. 1. However, this kind of periodic function has essentially never been used for proving the validity of approximate models (refer to the Introduction section). Yet, it is probably a much more realistic function than the square wave function when it comes to mimicking the actual variation in adsorbent surface concentration during periodic cycling. Hence, its use has the potential of providing more reliable conclusions about approximate model viability, as illustrated below and in subsequent discussions.

For the very strong adsorbate (most mathematically linear) system shown in Fig. 5, the curves from the QA and QN models essentially overlap the EN model for all three maximum surface concentrations. For the moderately strong (most mathematically nonlinear) adsorbate system shown in Fig. 6, the curve from the QA model only overlaps the EN model for the lower maximum surface concentration, with deviations clearly increasing as the maximum surface concentration increases; and the predictions are even worse for the PA model. Finally, for the somewhat strong adsorbate (moderately mathematically nonlinear) system shown in Fig. 7, the curve from the QA model only overlaps the EN model for the lower maximum surface concentration; but deviations begin to appear and grow as the maximum surface concentration increases. Since the reasons for these behaviors are the same as those reported for the square wave function, they are not repeated here. It suffices to state that in general the more mathematically linear the system the better the agreement between the approximate and exact models, and that in all cases it was again quite valid to assume κ and κ_0 to be constant under cyclic conditions with a sinusoidal wave function.

Triangular Wave Function

In this case, the surface concentration varies triangularly with time, as described by the periodic function given in Eq. (27) and shown in Fig. 1. During adsorption the surface concentration ψ_s increased linearly with time according to slope a while approaching $\psi_{s,\max}$. Then after time τ_P (the half-cycle time) had elapsed, the sign of a was changed to initiate desorption. During desorption the surface concentration ψ_s decreased linearly with time according to slope $-a$ while approaching zero. Figures 8, 9 and 10 respectively display the fractional uptake and release curves obtained from the approximate and exact models at maximum surface concentrations ($q_{s,\max}$) corresponding to 10, 40 and 70% of the adsorbent capacity (q_m) for the hexane-activated carbon, ethane-5A zeolite, and methane-activated carbon systems all at 298 K. The corresponding half-cycle times are given in Fig. 1.

The triangular wave function is the least abruptly changing surface boundary condition studied here, with it exhibiting a very gradual change over a cycle as shown in Fig. 1. It is surprising that this kind of periodic function apparently has never been used for proving the validity of approximate models (refer to the Introduction section). Yet, it is probably one of the more realistic functions that can be studied when it comes to mimicking the actual variation in concentration that the surface of an adsorbent particle is exposed to during periodic cycling in fixed bed adsorption processes. Hence, the use of this simple linear function has the potential of providing more reliable conclusions about approximate model viability, as illustrated below and in subsequent discussions.

For the very strong adsorbate system shown in Fig. 8, the curves from the QA and QN models essentially

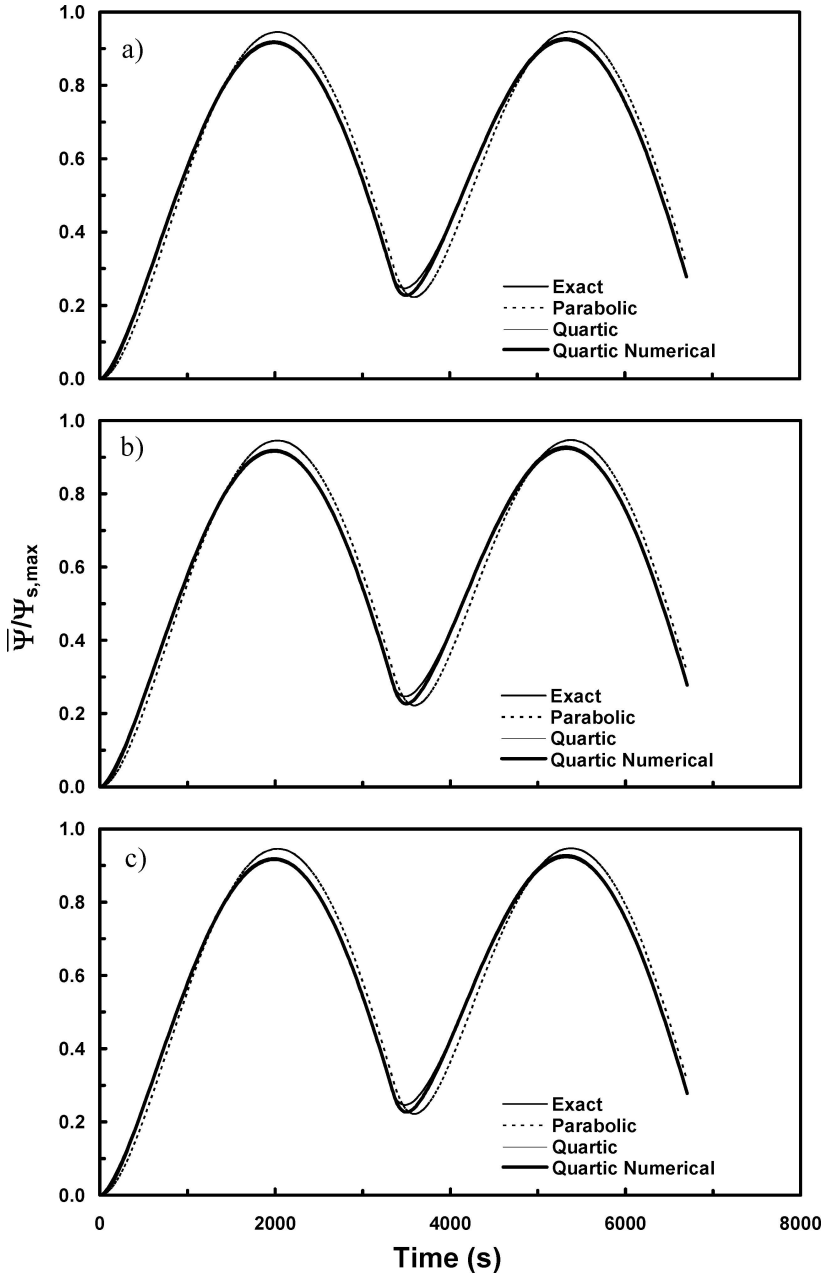

Figure 5. Comparison of fractional uptake curves obtained from various models for a sinusoidal change in the surface concentration for hexane-activated carbon at 298 K and $q_{s,\max}/q_m$ equal to (a) 0.1, (b) 0.4, and (c) 0.7.

overlap the EN model for all three maximum surface concentrations, with the PA model deviating only slightly from the EN model. For the moderately strong adsorbate system shown in Fig. 9, the predictions from the QA model agree very well with those from the EN model for all but the higher maximum surface concentration. But, even for this last case, the deviations are not too substantial. In all cases, the QA model does better than the PA model; and the QA model tends to agree with the QN model with slight deviations appearing for the higher maximum surface concentration. For the somewhat strong adsorbate system shown in Fig. 10, the curve from the QA and QN models again only overlap the EN model for the lower and intermediate

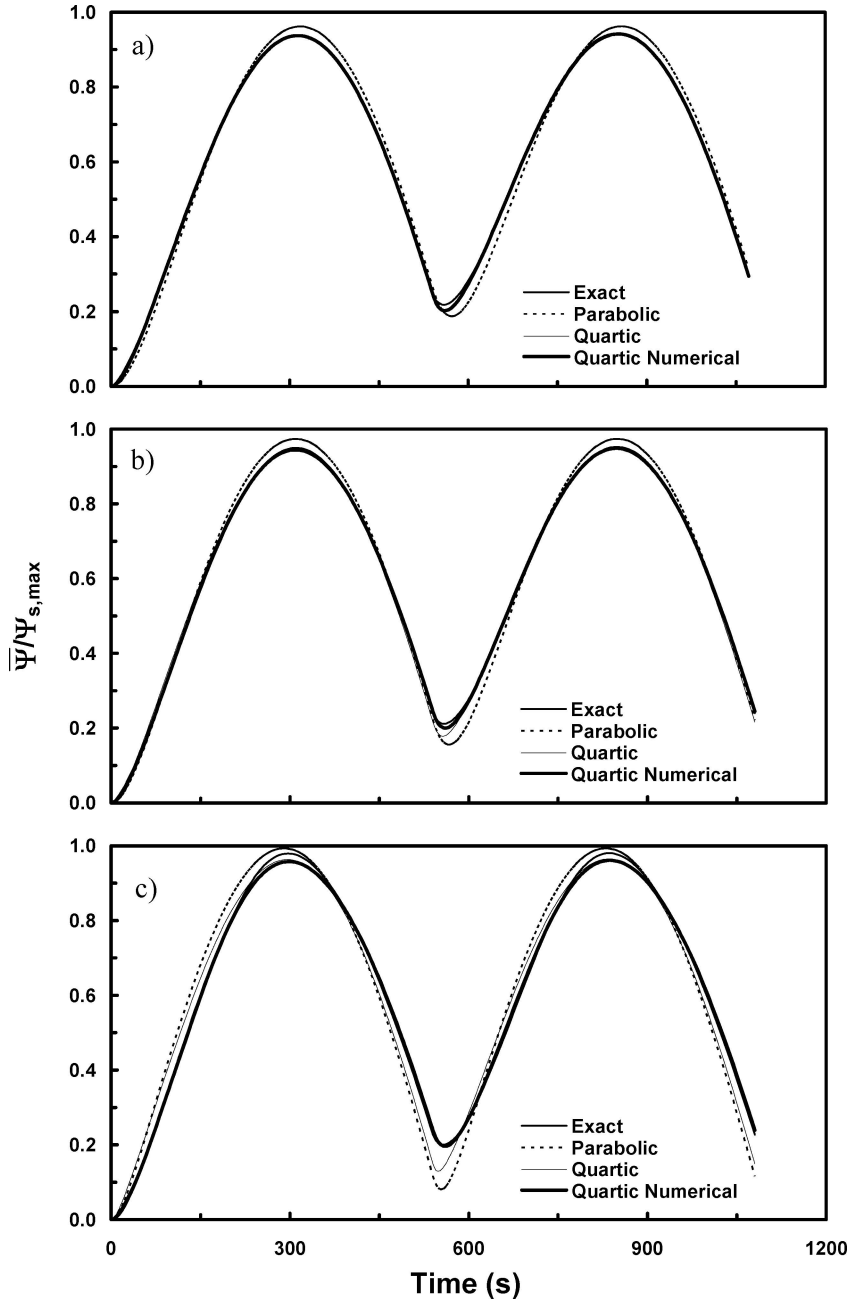

Figure 6. Comparison of fractional uptake curves obtained from various models for a sinusoidal change in the surface concentration for ethane-5A zeolite at 298 K and $q_{s,\max}/q_m$ equal to (a) 0.1, (b) 0.4, and (c) 0.7.

maximum surface concentrations; but slight deviations begin to appear at the higher maximum surface concentration; and the PA model, in all cases, exhibits the most deviation from the EN model. The reasons for these behaviors are essentially the same as those reported for the square wave function, so they are not repeated here. It is sufficient to note that the mathematical linearity of the system plays the decisive role in how well an approximate model agrees with the EN model. In addition, in all cases, it was valid to assume κ and κ_0 to

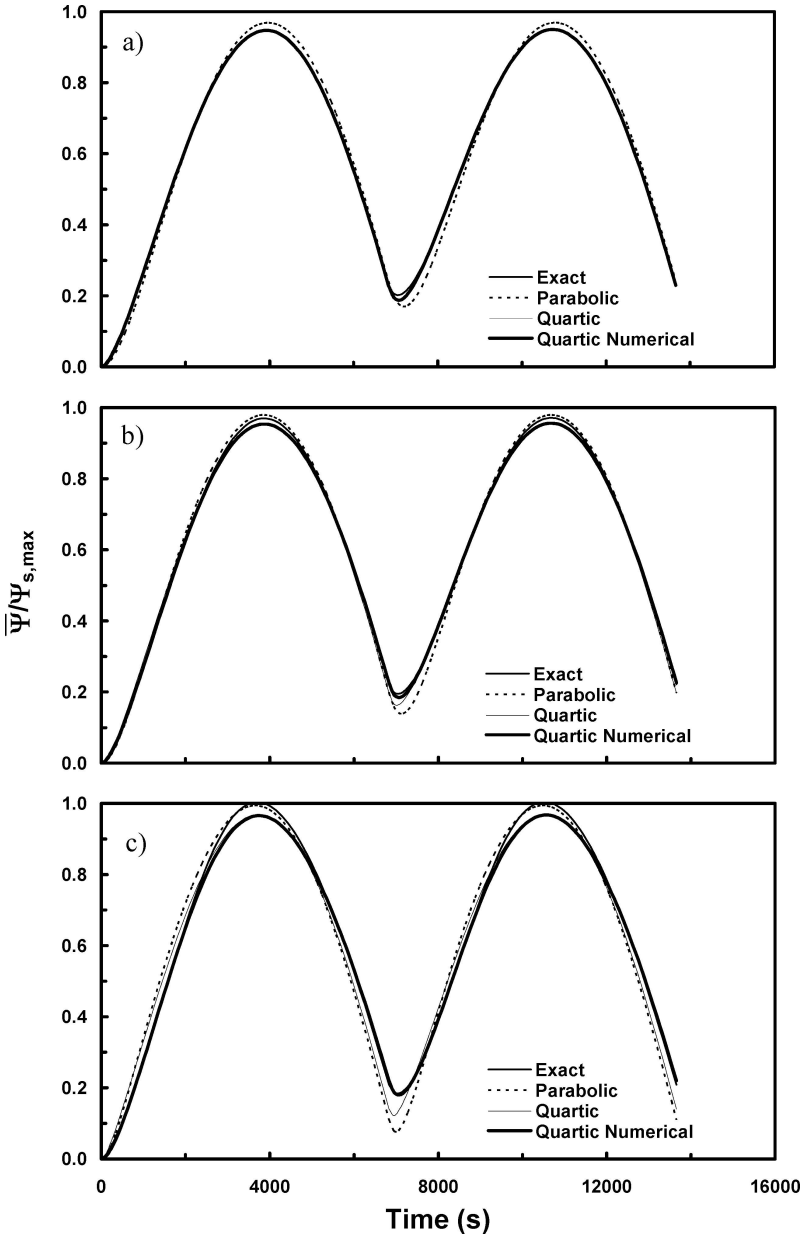

Figure 7. Comparison of fractional uptake curves obtained from various models for a sinusoidal change in the surface concentration for methane-activated carbon at 298 K and $q_{s,\max}/q_m$ equal to (a) 0.1, (b) 0.4, and (c) 0.7.

be constant under cyclic conditions with a triangular wave function.

Wave Function Form and Adsorbate-Adsorbent System Strength

In this section, the form of the wave function is compared and contrasted against the strength of each adsorbate-adsorbent system to elucidate how the approximate model predictability depends on both. A comparison of the results in Figs. 2 (square), 5 (sinusoidal), and 8 (triangular), shows that all three wave functions provide a fairly accurate depiction of the ability of the approximate models to predict the EN model for very strong adsorbate systems, like the hexane-activated carbon system. This result is unexpected,

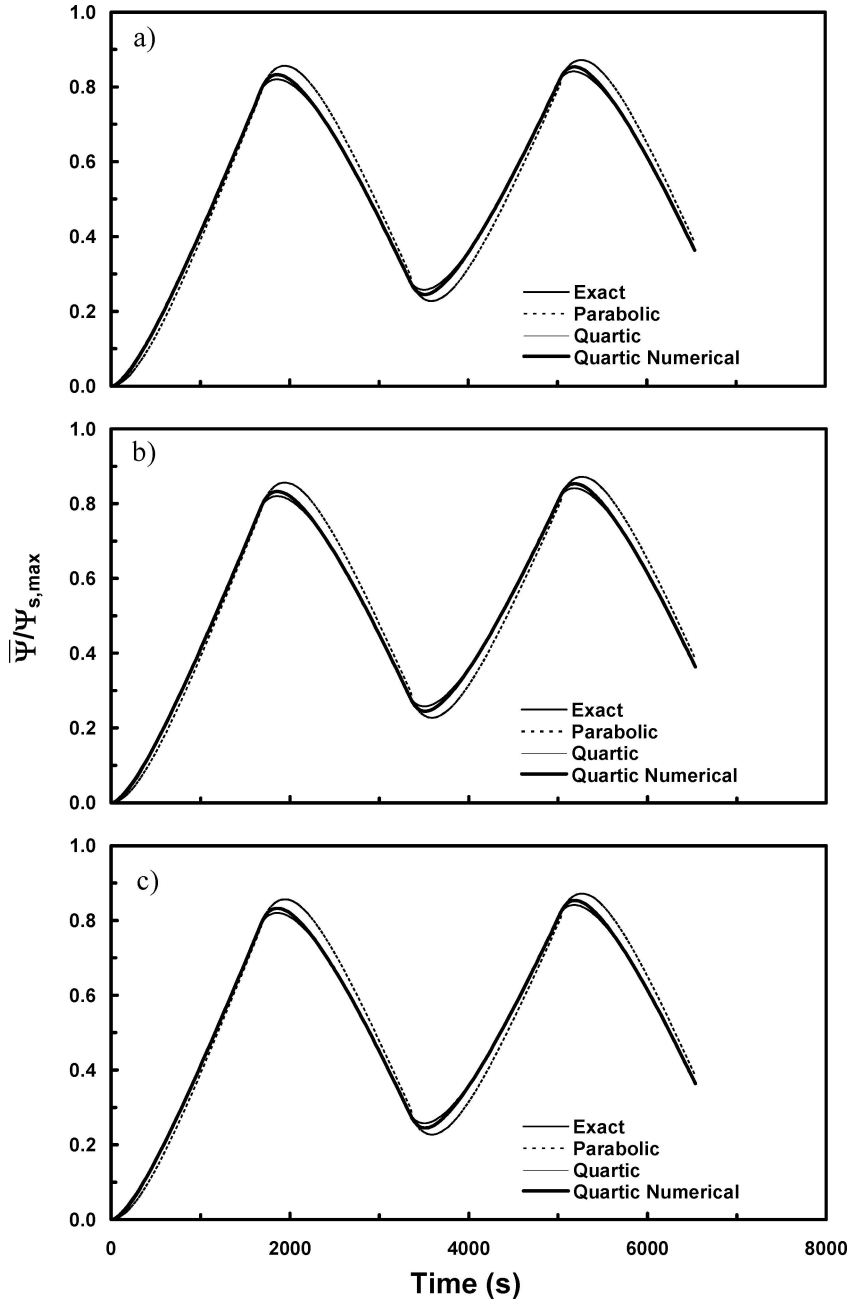

Figure 8. Comparison of fractional uptake curves obtained from various models for a triangular change in the surface concentration for hexane-activated carbon at 298 K and $q_{s,\max}/q_m$ equal to (a) 0.1, (b) 0.4, and (c) 0.7.

especially since an instantaneous step change in the surface concentration, resulting in a discontinuity with respect to time, may induce further nonlinearity into the system. The only plausible explanation again focuses on this very strong adsorbate, hexane-activated carbon system being the most mathematically linear system examined in this study. Hence, for very strong adsorbate systems with a high degree of mathematical

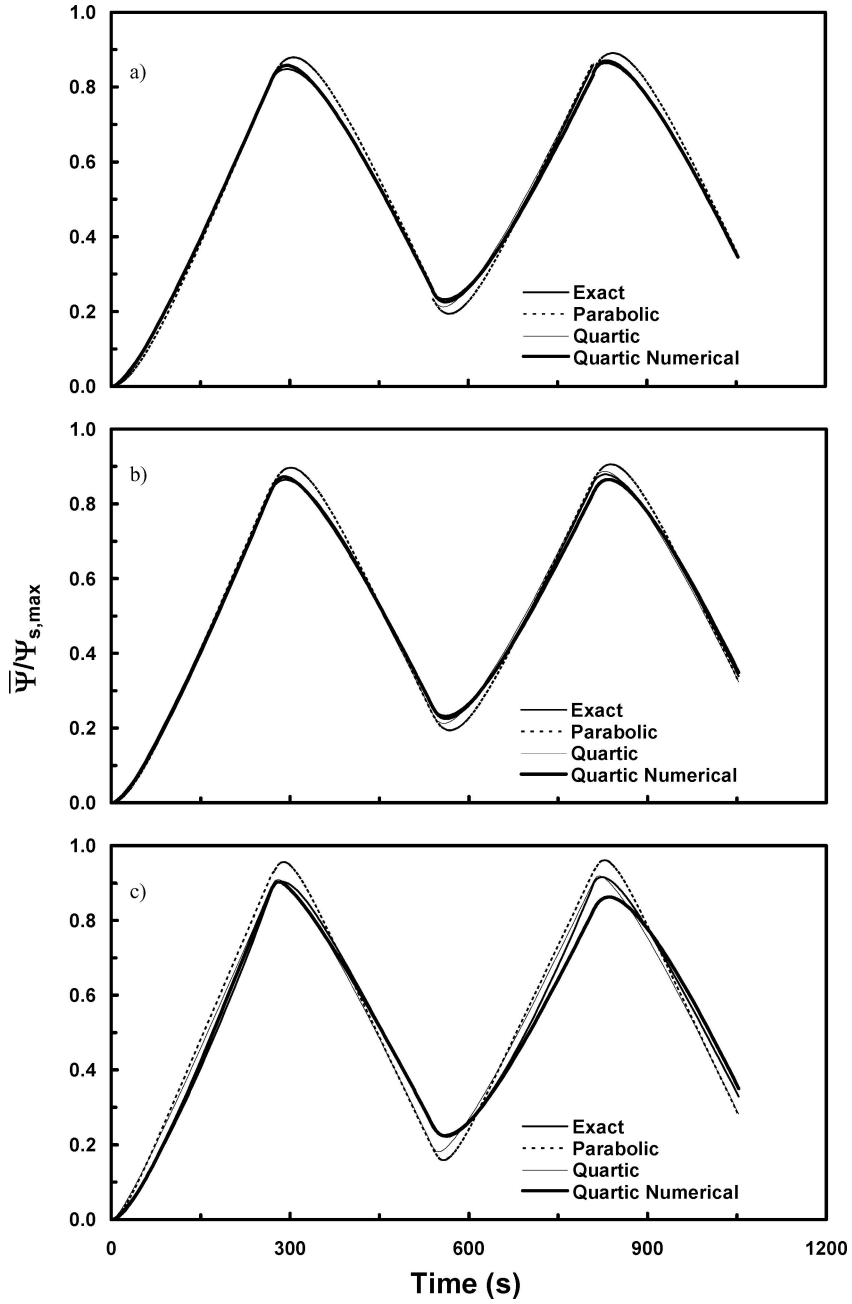

Figure 9. Comparison of fractional uptake curves obtained from various models for a triangular change in the surface concentration for ethane-5A zeolite at 298 K and $q_{s,\max}/q_m$ equal to (a) 0.1, (b) 0.4, and (c) 0.7.

linearity, it appears that any periodic wave function can be used to judge approximate model performance, even square wave functions. The situation is markedly different, however, for the two other adsorbate-adsorbent systems that exhibit more inherent mathematical nonlinearity.

For the ethane-5A zeolite system, an examination of Figs. 3 (square), 6 (sinusoidal), and 9 (triangular) indicates the triangular function to be the most forgiving with respect to the approximate model predictions agreeing with the EN model, followed by the sinusoidal and then the square wave function. These re-

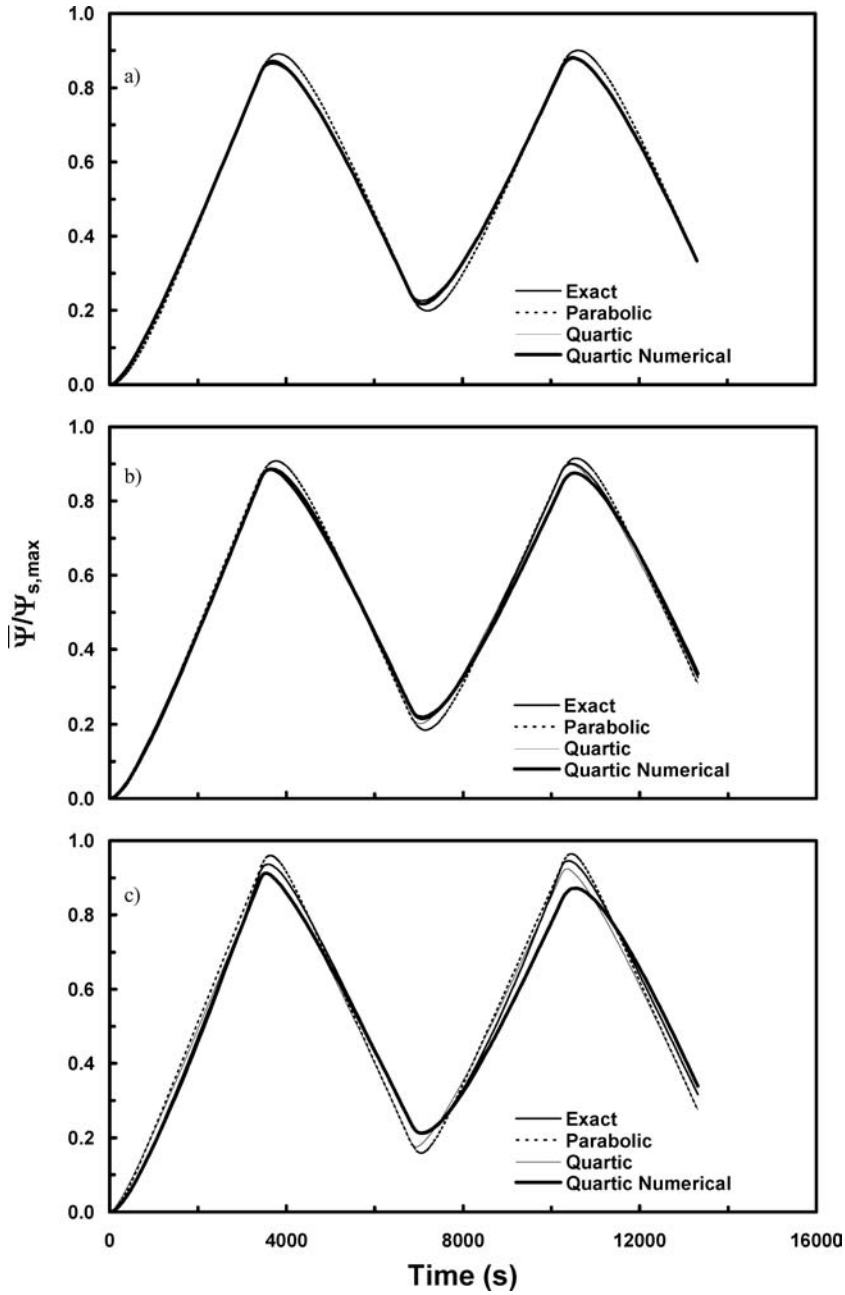

Figure 10. Comparison of fractional uptake curves obtained from various models for a triangular change in the surface concentration for methane-activated carbon at 298 K and $q_{s,\max}/q_m$ equal to (a) 0.1, (b) 0.4, and (c) 0.7.

sults are more in line with the expectations that the exclusive use of square wave functions may provide misleading or even erroneous results when it comes to approximate model validation. These results are also in line with the idea that the more gradual the change in the surface boundary condition, the more the boundary condition mimics long cycle time behavior, the better an approximate model may perform. This expected behavior is most likely due to this moderately strong adsorbate, ethane-5A zeolite system being the most

mathematically nonlinear system considered in this study. Further evidence supporting this conjecture is provided by the square, sinusoidal and triangular wave function results displayed in Figs. 4, 7 and 10 for the methane-activated carbon system. They reveal essentially the same behavior, but in this case it is for a somewhat strong adsorbate system that exhibits mathematical nonlinearity somewhere in between that associated with the other two systems. Hence, it is clear that except for very strong adsorbate systems that exhibit a high degree of mathematical linearity, as defined by Botte et al. (1998), the accuracy of an approximate model (or the reliability of a correlation for the cycle time dependence of the LDF mass transfer coefficient), may indeed depend on the type of wave function boundary condition utilized in the ensuing analysis. This important result is in agreement with that reported by Todd and Webley (2002).

Conclusions

The main objective of this study was to further validate the models developed previously by the authors under more realistic and diverse cycling conditions. These models, describing nonlinear adsorption and simultaneous pore and surface diffusion in a single particle, were based on intraparticle quartic and parabolic concentration profile approximations, and utilize the summation of the gas and adsorbed phases approach in the material balance formulations. The second objective was to expose the subtle and in some cases misleading differences in the predictive ability of the new approximate models that stem from the use of different periodic wave functions for describing the surface boundary condition. Periodic square, sinusoidal and triangular wave functions were used to more accurately represent the periodic boundary conditions that the external surface of an adsorbent particle may be exposed to during repeated adsorption and desorption cycles in a fixed bed adsorber. Analytical periodic solutions that describe the adsorbate uptake during adsorption and release during desorption were obtained for all three periodic wave functions, and for both the quartic and parabolic profile approximations.

Three different adsorbate-adsorbent systems (hexane-activated carbon at 298 K, ethane-5A zeolite at 298 K, and methane-activated carbon at 298 K) that respectively represent very strong, moderately strong, and somewhat strong adsorbate-adsorbent systems were used to examine the accuracy of the new approximate models under the diverse cycling conditions. The hexane-activated carbon was the most mathematically linear system, followed by the methane-activated carbon system, and then the ethane-5A zeolite system. For each adsorbate-adsorbent system, three maximum surface concentrations, corresponding to 10, 40 and 70% of the adsorbent capacity, were studied in each case to investigate the effect of isotherm nonlinearity.

By comparing the fractional periodic uptakes and releases obtained from both models against the exact numerical solution, the superiority of the quartic model over the parabolic model was clearly demonstrated, with excellent agreement between the quartic and exact models obtained in many instances. The quartic model always outperformed the parabolic model; and in general, it exhibited reasonably accurate predictions even at short times during the initial uptakes and releases of adsorbate for all three adsorbate-adsorbent systems at all three maximum surface concentrations. However, the accuracy of the predictions depended on the wave function and the adsorbate-adsorbent system. The best predictions were exhibited by the functions that changed more gradually with time, i.e., the more realistic sinusoidal and triangular functions; the worst predictions were exhibited by the function that changed most abruptly with time, i.e., the more unrealistic square wave function. Also, the accuracies of the predictions from the quartic and parabolic models depended on the mathematical nonlinearity of the adsorbate-adsorbent system, with accuracies improving greatly with mathematical linearity. Similarly, the predictions generally became less accurate as the maximum surface concentration increased, an effect related more directly to isotherm nonlinearity. These results show very clearly that the judged accuracy of the approximate models depends not only on the wave function boundary condition but also and distinctly on the degree of linearity of the adsorbate-adsorbent system.

Overall, these results collectively exemplify the importance of comparing the predictive ability of new approximate models that describe intraparticle transport (or even time dependent LDF mass transfer coefficient correlations) under more diverse yet realistic cycling conditions than are typically utilized in the literature, which has been dominated by the square wave function. Except for very strong adsorbate systems that exhibit a high degree of mathematical linearity, the type of wave function boundary condition chosen to determine approximate model accuracy (or cycle time dependence

of the LDF mass transfer coefficient) may have a profound effect on the outcome of the analysis. When in doubt, it may be prudent to examine three or more different periodic wave function boundary conditions, such as square, sinusoidal and triangular (as done here), to gain a more complete and unbiased perspective on the predictive ability of a new approximate model.

Nomenclature

a	Slope of the ramp in the triangular wave function, Eq. (46)
b	Langmuir isotherm parameter, m^3/kg
b'	Dimensionless Langmuir isotherm parameter, $bc_{s,\max}$
C	Dimensionless gas phase concentration in the pores of the adsorbent particle, $c/c_{s,\max}$
C_o	Dimensionless gas phase concentration at the center of the adsorbent particle, $c_o/c_{s,\max}$
C_s	Dimensionless gas phase concentration at the surface of the adsorbent particle, $c_s/c_{s\cdot\max}$
c	Concentration in the pores of the adsorbent particle, kg/m^3
$c_{\mathrm{s.max}}$	Maximum concentration at the external surface of the adsorbent particle, taking on values of 10, 40 and 70% of the adsorbent capacity q_m, kg/m^3
D_g	Gas phase (pore) diffusivity, m^2/s
D_a	Adsorbed phase (surface) diffusivity, m^2/s
j_1	Function defined by Eq. (29)
j_2	Function defined by Eq. (30)
M_t	Total uptake by the adsorbent particle at time t, kg/m^3
M_∞	Total uptake by the adsorbent particle at infinite time, kg/m^3
N_ξ	Dimensionless total flux into the adsorbent particle at radial position ξ
Q	Dimensionless adsorbed phase concentration in the adsorbent particle, $\gamma q/c_{s,\max}$
Q_o	Dimensionless adsorbed phase concentration in equilibrium with the gas at the center of the adsorbent particle, $\gamma q_o/c_{s\cdot\max}$
Q_s	Dimensionless adsorbed phase concentration in equilibrium with gas surrounding the adsorbent particle, $\gamma q_s/c_{s,\max}$
Q_m	Dimensionless Langmuir isotherm parameter, $\gamma q_m/c_{s,\max}$
q	Adsorbed phase concentration in the adsorbent particle, kg/kg
q_m	Langmuir isotherm parameter and a measure of adsorbent capacity, kg/kg
$q_{s,\max}$	Adsorbed phase concentration in equilibrium with the maximum gas phase concentration surrounding the adsorbent particle, kg/kg
r	Radial coordinate, m
R_p	Radius of adsorbent particle, m
t	Time, s

Greek Letters

ε_p	Void fraction of adsorbent particle
ρ_p	Density of adsorbent particle, kg/m^3
γ	Ratio of particle density to intraparticle void fraction, ρ_p/ε_p
λ	Ratio of adsorbed phase (surface) diffusivity to gas phase (pore) diffusivity, D_a/D_g
κ	Function defined at the adsorbent particle surface, Eq. (16)
κ_0	Function defined at the adsorbent particle center, Eq. (19)
μ	Function defined by Eq. (31)
	Dimensionless time, $D_g t/R^2$
τ_i	Dimensionless time at the beginning of each half cycle
τ_P	Dimensionless half cycle time for each uptake and release cycle
ξ	Dimensionless radial distance, r/R_P
ψ	Dimensionless sum of the adsorbate concentrations in the gas and adsorbed phases, C + Q
Ψ_o	Dimensionless sum of the adsorbate concentrations in the gas and adsorbed phases at the center of the particle
$\Psi_{o,i}$	Dimensionless sum of the adsorbate concentrations in the gas and adsorbed phases at the center of the particle at the beginning of each half cycle
$\Psi_{s,i}$	Dimensionless maximum sum of the adsorbate concentrations in the gas and adsorbed phases at the surface of the particle at the beginning of each half cycle
$\Psi_{s,f}$	Dimensionless maximum sum of the adsorbate concentrations in the gas and adsorbed phases at the surface of the particle at the end of each half cycle

$\bar{\Psi}$	Dimensionless average sum of the adsorbate concentrations in the gas and adsorbed phases
$\bar{\Psi}_i$	Dimensionless average sum of the adsorbate concentrations in the gas and adsorbed phases at the beginning of each half cycle
$\psi_{s,\max}$	Dimensionless maximum sum of the adsorbate concentrations in the gas and adsorbed phases at the surface of the particle corresponding to $c_{s,\max}$
ω	Angle or phase shift of the sinusoidal function, Eq. (36)

Acknowledgments

Financial support provided by the MeadWestvaco Charleston Research Center and the Separations Research Program at the University of Texas at Austin is greatly appreciated.

References

Botte, G.G., R. Zhang, and J.A. Ritter, "On the Use of Different Parabolic Concentration Profiles for Non-linear Adsorption and Diffusion in a Single Particle," *Chem. Eng. Sci*., **53**, 4135–4146 (1998).

Botte, G.G., R. Zhang, and J.A. Ritter, "New Approximate Model for Nonlinear Adsorption and Concentration Dependent Surface Diffusion in a Single Particle," *Adsorption*, **5**, 375–382 (1999).

Buzanowski, M.A. and R.T. Yang, "Extended Linear Driving Force Approximation for Intraparticle Diffusion Rate Including Short Times," *Chem. Eng. Sci.*, **44**, 2683–2689 (1989).

Buzanowski, M.A. and R.T. Yang, "Approximations for Intraparticle Diffusion Rates in Cyclic Adsorption and Desorption," *Chem. Eng. Sci.,* **46**, 2589 (1991).

Do, D.D. and P.L.J. Mayfield, "A New Simplified Model for Adsorption in a Single Particle," *AIChE J*. **33**, 1397–1400 (1987).

Do. D.D. and R. Rice, "Validity of the Parabolic Profile Assumption in Adsorption Studies," *AIChE. J*., **32**, 149–154 (1986).

Do. D.D. and R. Rice, "Revisiting Approximate Solutions for Batch Adsorbers: Explicit Half time," *AIChE. J*., **41**, 426–429 (1995).

Do, D.D. and T.S. Nguyen, "A Power Law Adsorption Model and Its Significance," *Chem. Eng. Comm*., **72**, 171–185 (1988).

Gadre, S.A. and J.A. Ritter, "New Analytical Solution for Nonlinear Adsorption and Diffusion in a Single Particle," *Chem. Eng. Sci*., **57**, 1197–1204 (2002a).

Gadre, S.A. and J.A. Ritter, "New Model for Non-Linear Adsorption and Diffusion Based on a Quartic Concentration Profile Approximation," *Ind. Eng. Chem. Res*., **41**, 4353–4361 (2002b).

Glueckauf, E., "Theory of Chromatography 10: Formulae for Diffusion into Spheres and Their Application to Chromatography," *Trans. Faraday Soc*., **51**, 1540–1551 (1955).

Li, Z. and R.T. Yang, "Concentration Profile for Linear Driving Force Model for Diffusion in a Particle," *AIChE J*., **45**, 196–200 (1999).

Liaw, C.H., J.S.P. Wang, R.H. Greenkorn, and K. C. Chao, "Kinetics of Fixed-Bed Adsorption: A New Solution," *AIChE J*., **54**, 376–381 (1979).

Rodrigues A.E. and M.M. Dias, "Linear Driving Force Approximation in Cyclic Adsorption Processes: Simple Results from System Dynamics based on Frequency response Analysis," *Chem. Eng. Sci*., **37**, 489–502 (1998).

Serbezov A. and S.V. Sotirchos, "On the Formulation of Linear Driving Force Approximations for Adsorption and Desorption of Multicomponent Gaseous Mixtures in Sorbent Particles," *Sep. Purif. Tech*., **24**, 343–367 (2001).

Sircar, S. and J.R. Hufton, "Why Does the Linear Driving Force Model for Adsorption Kinetics Work?" *Adsorption*, **6**, 137–147 (2000).

Todd, R.S. and P.A. Webley, "Limitations and the LDF/Equimolar Counterdiffusion Assumption for Mass Transport within Porous Adsorbent Pellets," *Chem. Eng. Sci*., **57**, 4227–4242 (2002).

Tomida, T. and B.J. McCoy, "Polynomial Profile Approximation for Intraparticle Diffusion," *AIChE J.,* **33**, 1908–1911 (1987).

Yao. C. and C. Tien, "Approximations of Uptake Rate of Spherical Adsorbent Pellets and Their Applications to Batch Adsorption Calculations. *Chem. Eng. Sci.*, **48**, 187–197 (1993).

Zhang, R., and J.A. Ritter, "New Approximate Model for Nonlinear Adsorption and Diffusion in a Single Particle," *Chem. Eng. Sci*., **52**, 3161–3172 (1997).